PERGAMON

Computers & Geosciences 25 (1999) 963–978

COMPUTERS & GEOSCIENCES

The scale invariant generator technique for quantifying anisotropic scale invariance

G.M. Lewis[a, 1], S. Lovejoy[a,*], D. Schertzer[b], S. Pecknold[a]

[a]*Department of Physics, McGill University, 3600 University St., Montréal, Que., Canada H3A 2T8*
[b]*LMD (CNRS) Boite 99, Université P.&M. Curie, 4 Pl. Jussieu, Paris 75252 Cedex 05, France*

Received 14 October 1997; received in revised form 25 June 1998; accepted 20 August 1998

Abstract

Scale invariance is rapidly becoming a new paradigm for geophysics. However, little attention has been paid to the anisotropy that is invariably present in geophysical fields in the form of differential stratification and rotation, texture and morphology. In order to account for scaling anisotropy, the formalism of generalized scale invariance (GSI) was developed. Until now there has existed only a single fairly ad hoc GSI analysis technique valid for studying differential rotation.

In this paper, we use a two-dimensional representation of the linear approximation to generalized scale invariance, to obtain a much improved technique for quantifying anisotropic scale invariance called the scale invariant generator technique (SIG). The accuracy of the technique is tested using anisotropic multifractal simulations and error estimates are provided for the geophysically relevant range of parameters. It is found that the technique yields reasonable estimates for simulations with a diversity of anisotropic and statistical characteristics. The scale invariant generator technique can profitably be applied to the scale invariant study of vertical/horizontal and space/time cross-sections of geophysical fields as well as to the study of the texture/morphology of fields.

Keywords: Anisotropy; Scale invariance; Analysis technique; Texture; Multifractal

1. Introduction

The use of scale invariance in the study of geophysics — even if only implicitly in the form of fractal geometry — is becoming widespread. Unfortunately, existing scale invariant models and analysis techniques (whether mono or multifractal) usually assume self-similarity (hence isotropy). In contrast to these isotropic assumptions and models, geophysical fields are generally highly anisotropic. For example, in the atmosphere, ocean and earth interior, they are differentially stratified due to gravity. Furthermore, clouds, ridges in sea ice, fault planes in earthquakes and mountain ranges in topography — to name a few — all have scale-dependent preferred directions arising from the Coriolis force, external stresses, or other boundary conditions which lead to differential rotation. The full scope of the scale-invariant symmetry principle has therefore been drastically underestimated; perhaps an extreme example being the atmosphere, where the use of outmoded isotropic scaling notions has lead to the prediction of a "meso-scale gap"

* Corresponding author. Fax: +1-514-398-8434.
E-mail address: lovejoy@physics.mcgill.ca (S. Lovejoy)
[1] Present address. Department of Mathematics, University of British Columbia, Vancouver, BC, Canada.

0098-3004/99/$ - see front matter
PII: S0098-3004(99)00061-8

between the large and small scales which is not compatible with modern scaling analyses or theories (see Lovejoy et al., 1993).

Scale invariance is a symmetry respected by systems whose large and small scales are related by a scale changing operation involving only the scale ratio: they have no characteristic size. As with the familiar symmetries associated with energy and momentum conservation, the scaling symmetry must a priori be assumed to hold. Only when a specific symmetry breaking mechanism can be shown to exist should one invoke the existence of fundamental length scales. While it is true that in self-similar scaling small structures look the same as large ones, this is no longer true in anisotropic scaling, hence phenomenological classifications of structures can be quite misleading. Although many geophysical fields exhibit no symmetry-breaking mechanism over a wide range of scales, for purely phenomenological reasons (i.e. phenomena *look* different at different scales) a scale bound/nonscaling approach is often adopted; e.g. a phenomenological school exists in meteorology which hypothesizes the existence of different dynamical mechanisms every factor of two or so in scale — in spite of the fact that the underlying (Navier–Stokes) equations are scaling between a small viscous scale (of the order of a mm) and a large scale of planetary dimensions. Furthermore, since they are also scaling, boundary conditions (e.g. topography, Lovejoy and Schertzer, 1990; Lavallée et al., 1993) will not break the scaling.

Not only are the usual theoretical scaling notions isotropic, so are the corresponding data analysis techniques. For example, a common tool used to study geophysical scale invariance is the isotropic energy spectrum, $E(k)$, (where $k=|\mathbf{k}|$ and $\mathbf{k}$ is the wave number), which is obtained by angle integrating (i.e. integrating out) the angular energy density. If a field is isotropic and scaling, then $E(k)\sim k^{-\beta}$, where β is the scale invariant spectral exponent. Therefore, the anisotropy of a scaling field (if it is not extreme) may be "washed-out" by the smoothing effect of the integration. Thus, a power-law isotropic energy spectrum can indicate approximate scaling without implying isotropy (see Lovejoy et al., 1993, for a discussion of this in cloud radiances). The same is true of box-counting and other fractal or multifractal analysis techniques which use similarly shaped boxes or circles at different scales, hence (implicitly) isotropic scale changes. On the other hand, an apparent break in the scaling of an isotropic spectrum or other statistic may be spurious; it may simply imply *anisotropic* scaling. Similarly, spectra of one-dimensional cross sections of anisotropic processes may also show spurious breaks in the scaling.

Although geophysical fields are a priori scale invariant, there is usually no reason to assume a specific type of anisotropy (e.g. self-affinity); quite general forms of scale invariance must be considered. In several papers, Schertzer and Lovejoy (1983, 1984, 1985, 1987, 1989, 1991) present a formalism called Generalized Scale Invariance (GSI), which defines the notion of scale in anisotropic scaling systems. The physical motivation for GSI is that the dynamics should determine the appropriate notion of scale; it should not be imposed from without.

Other researchers have seen the need for studying the anisotropy of geophysical fields. Fox and Hayes (1985), VanZandt et al. (1990), and Pilkington and Todoeschuk (1993) independently proposed the introduction of different scaling exponents in different directions. Although at first sight this is appealing, it turns out to be quite incompatible with a scaling generation of anisotropy. For the mechanism to be independent of the absolute scale, and to depend only on the scale ratio (relative scale), the scale changes must satisfy group properties (see Section 2). Since this is not the case for this approach, any underlying dynamics will be fundamentally dependent, rather than independent, of size.

Recently, starting in the turbulence literature, an idea closely related to GSI has been in vogue: extended self-similarity (ESS). GSI uses an anisotropic notion of scale which is physically determined by the dynamics (especially the differential rotation and stratification of structures). Similarly, ESS uses a scale defined by the statistics (in turbulence, the third order velocity structure function), in this case, the idea is to (somewhat) take into account the dissipation which destroys the scaling with respect to the usual scale notions. In both cases, rather than using an academic (Eulerian) scale, one attempts to let them be determined by the dynamics. See Schertzer et al. (1997) for further discussion of the relation of ESS to GSI.

To date, the only data analysis technique which can handle both differential rotation and stratification is the Monte-Carlo differential rotation method (Pflug et al., 1991 and 1993; Lovejoy et al., 1992; see also Lovejoy et al. (1987) for a discussion of the anisotropic "elliptical-dimensional sampling technique"). However, this technique has many problems (discussed later) and the new scale invariant generator (SIG) technique outlined here is a considerable improvement.

SIG quantifies anisotropic scale invariance by estimating the GSI parameters. It was developed to study the scaling of the spectral energy density in geophysical phenomena (yet with little effort it can be more generally applied). The scaling is a statistical property, therefore large data sets (large ranges of scales) are needed to ensure accurate results. For this purpose, satellite images of geophysical phenomena are often studied. Because of these large data sets, a major challenge of developing an analysis technique is to make it

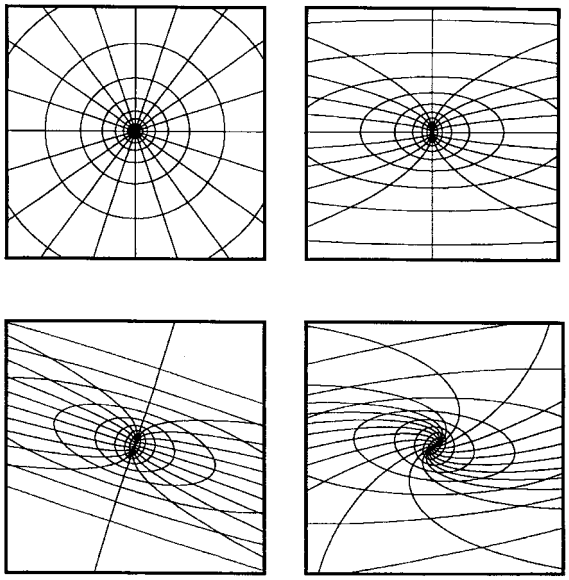

Fig. 1. Examples of balls and trajectories for linear GSI (see ++Section 2.2) with sphero-scale. Trajectories are "radial" lines and frontiers of balls are ellipses (second order polynomials). Top left: isotropic case: $c = 0.0$, $f = 0.0$, $e = 0.0$. Top right: self-affine case: $c = 0.35$, $f = 0.0$, $e = 0.0$. Bottom left: rotated self-affine case: $c = 0.35$, $f = 0.25$, $e = 0.0$. Bottom right: case with rotation of balls: $c = 0.35$, $f = 0.25$, $e = 0.6$. $d = 1$ for all cases. See ++Section 2.2 for definition of d, c, f and e.

efficient. The previous analysis technique was adequate to show the applicability of GSI to actual cloud radiances. However, in order to realize the full potential of GSI, it is necessary to develop a technique which can estimate the GSI parameters quickly and with confidence for a variety of geophysical fields. Therefore, in this paper we concentrate on proving the accuracy of the SIG technique by applying it to simulated fields with known GSI parameters (various anisotropy) and with various statistical properties. More details can be found in Lewis (1993).

We begin with a brief description of generalized scale invariance and its application to the study of geophysical fields. Following this is a description of the analysis technique and a discussion of its accuracy.

2. Generalized scale invariance

2.1. General features

In general, a scale invariant system needs a way of identifying vectors of the same scale (size) and it needs a way of measuring the scale of these vectors. It also needs a way of relating the different scales in such a way that a characteristic size is not introduced to the system. Usual (isotropic) scale invariant systems use the length of vectors to determine their scale and therefore vectors of equal length are of the same scale. Vectors of different scales are related by a magnification (scaling) factor which depends on the ratio of the lengths of the vectors. See top left of Fig. 1.

Generalized scale invariance (GSI) moves away from this restrictive case, allowing more general concepts of scale and scale changing operations. GSI is a formalism which states the most general conditions under which a system can be scale invariant. A GSI system requires three elements:

1. The unit ball, B_1, which defines the unit vectors. In general, B_1 will be defined by an implicit equation:

$$B_1 = \{\mathbf{x}|\, f_1(\mathbf{x}) < 1\}; \quad \partial B_1 = \{\mathbf{x}|\, f_1(\mathbf{x}) = 1\} \tag{1}$$

   where ∂B_1 is the "frontier of the unit ball", and f_1 (a function of position, $\mathbf{x}$; bold will denote vector quantities) is the "scale function". If there is a scale where all the vectors are of the same length, the ball will be isotropic (e.g. a circle or sphere) and the corresponding scale is called the "sphero-scale".
2. The scale changing operator T_λ which transforms the scale of vectors by scale ratio λ. T_λ depends only on the scale ratio: it involves no characteristic size. This implies that T_λ is a one parameter multiplicative (semi) group: $T_\lambda = \lambda^{-G}$, where G is the generator. Although the inverse operator $T_\lambda^{-1} = T_{\lambda^{-1}}$ need not exist, here we will only consider linear GSI (G is a matrix; see ++Section 2.2), and an inverse will generally exist (T_λ is a group as opposed to a semigroup). For isotropic systems, G is the identity. It can be seen that even when only linear GSI is considered, GSI is able to describe much richer behaviors.

Given elements 1 and 2, we can now define a family of open balls B_λ:

$$\forall x: f_\lambda(\mathbf{x}) = f_1(T_\lambda^{-1}\mathbf{x}); \quad B_\lambda = \{\mathbf{x}; f_\lambda(\mathbf{x}) < 1\}. \tag{2}$$

Since the triangle inequality is not necessarily satisfied, we are generally not dealing with true norms. It is nevertheless often convenient to use the "norm" notation:

$$\|\mathbf{x}\| = \{\lambda|\mathbf{x} \in \partial B_\lambda\} \tag{3}$$

hence:

$$\|T_\lambda \mathbf{x}\| = \lambda^{-1}\|\mathbf{x}\|. \tag{4}$$

Alternatively, Eq. (3) means that $f_\lambda(\mathbf{x}) = 1 \Leftrightarrow \|\mathbf{x}\| = \lambda$ (all vectors, $\mathbf{x}$, which lie on the same ∂B have the same scale). Note that since ∂B are not generally circles or spheres, the usual vector

norm cannot be used. Thus, B_λ identify vectors of the same scale and T_λ relates the vectors of different scales. As yet, however, the vectors have not been given an absolute size; they have only been compared to the unit ball. Thus, generally, the last element is needed.

3. A measure of size: The vectors can be associated with a size by defining a measure, ϑ, that assigns a unique positive real number, monotonically increasing from low to high scales, to every ball, B. For example, we may use the volume of the balls raised to any positive power to define our measure of scale. For GSI in two dimensions, it is convenient to use the square root of the area of the ball. In some cases, for example where there is strong overall stratification such as the vertical cross-section of the atmosphere, it may be more convenient to use the horizontal extent as a measure of the size (see Schertzer and Lovejoy, 1985). Note that the unit ball implies $\lambda = 1$, which does not refer to an absolute scale. Thus, the unit ball is simply the ball to which all other balls are compared. Alternatively, λ can be thought of as a "normalized" scale.

In order for the scale to be uniquely defined (each vector related to only one scale), we must have $B_{\lambda_1} \subset B_{\lambda_2}$ whenever $\lambda_1 > \lambda_2$. If the balls are defined by the function f_λ (Eq. (2)), this condition implies

$$\frac{\partial f_\lambda}{\partial \lambda} > 0 \quad \forall \mathbf{x}. \tag{5}$$

Eq. (5) ensures that the frontiers of the balls do not cross (since $f_\lambda(\mathbf{x}) = 1$ and $f_{\lambda+\delta\lambda}(\mathbf{x}) = 1$ will then have no simultaneous solution for small $\delta\lambda$). This is generally a nontrivial technical constraint on the GSI system.

Rather than consider the dilation/contraction of the balls, one may invoke the idea of a trajectory. If one vector is related to another by T_λ (e.g. $\mathbf{x}_2 = T_\lambda \mathbf{x}_1$, for some λ; i.e. $\mathbf{x}_2$ is a factor λ reduction of vector $\mathbf{x}_1$), then they lie on the same trajectory. Starting at the unit ball, and varying λ from 1 to ∞ (in $\mathbf{x}_\lambda = T_\lambda \mathbf{x}_1$), a complete trajectory can be traced out (see Fig. 1). All the trajectories are obtained by systematically starting on all vectors on the frontier of the unit ball. The condition that the scale be uniquely defined implies that the eigenvalues of G must have negative real part. Each vector of the field is a member of one and only one trajectory. The use of trajectories rather than balls has the key advantage (exploited here) that every G generates a unique set of trajectories *irrespective of the unit ball*. In practice this will mean that we can first determine G, and then B_1.

2.2. Properties of linear GSI in two-dimensional real space

Since we are assuming statistical homogeneity (see Section 2.3), T_λ will be independent of position and thus will be a linear transformation. Therefore, linear generalized scale invariance (Schertzer and Lovejoy, 1985; Lovejoy and Schertzer, 1985) will be used. In linear GSI, G is a matrix and thus has D^2 parameters (where D is the dimension of space). Note that many geophysical fields of interest are not homogeneous (e.g. atmospheric motions, since the Coriolis force is a function of latitude) and hence linear GSI is not exact. However, in principle, it is possible to consider a series of sub-regions of the field, where the linear GSI approximation will hold over a sufficiently large range of scales.

The simplest nontrivial anisotropic system is two-dimensional; this is also of practical significance, since satellite radiances typically have $D = 2$. Hence, here we take G to be a 2×2 matrix. G will be written as a linear combination of the basis of two-dimensional matrices (pseudo-quaternions, Schertzer and Lovejoy, 1985; Lovejoy and Schertzer, 1985):

$$G = d\mathbf{1} + c\mathbf{K} + f\mathbf{J} + e\mathbf{I}, \tag{6}$$

where:

$$\mathbf{1} = \begin{pmatrix} 1 & 0 \\ 0 & 1 \end{pmatrix}, \quad \mathbf{K} = \begin{pmatrix} 1 & 0 \\ 0 & -1 \end{pmatrix}, \quad \mathbf{J} = \begin{pmatrix} 0 & 1 \\ 1 & 0 \end{pmatrix}, \quad \mathbf{I} = \begin{pmatrix} 0 & 1 \\ -1 & 0 \end{pmatrix}. \tag{7}$$

Thus

$$G = \begin{pmatrix} d+c & f+e \\ f-e & d-c \end{pmatrix}. \tag{8}$$

Written as such, not only can a functional form of T_λ be found, but the parameters take on a more obvious interpretation: d is a measure of overall contraction, c is a measure of the relative scaling of the two coordinate axes, f is a reflection across a line diagonal to the axes and e is a measure of rotation (see Fig. 1). We will choose $d = 1$. This corresponds to choosing the square root of the area of the balls as the measure of scale, ϑ. A different choice of power of the area will correspond to a different d.

Since the balls may be of any shape, it may require an infinite number of parameters to describe them. Therefore, for the purpose of analysis, it is necessary to approximate the balls (by approximating f_λ). In linear GSI, T_λ is simply a linear transformation and since we study the spectral energy density (see ++Section 2.3) our data will be invariant under the inversion

$\mathbf{x} \rightarrow -\mathbf{x}$. It is therefore natural to approximate f_1 using even order polynomials since their form is invariant under linear transformations and inversions. This ensures that f_λ can be described in the same form as f_1. The simplest example of such polynomials are the quadratic forms, characterized by the equation

$$f_1(\mathbf{x}) = \mathbf{x}^T \mathbf{A}_1 \mathbf{x} = 1. \tag{9}$$

In two dimensions, $\mathbf{A}_1 = \begin{pmatrix} A_{00} & A_{01} \\ A_{01} & A_{11} \end{pmatrix}$ and the vectors, $\mathbf{x} = \begin{pmatrix} x \\ y \end{pmatrix}$, which satisfy this equation, lie on the frontier of the unit ball. Only ellipses are permitted since hyperbolae and parabolae do not form closed curves, giving the constraints A_{00}, $A_{11} > 0$ and $A_{00}A_{11} - A_{01}^2 > 0$ (note that since one can nevertheless define an inside and an outside, hyperbolae and parabolae may find applications elsewhere). See ++Appendix A for a derivation of the scale uniqueness condition for the quadratic case. It was found in the study of actual geophysical fields (clouds and sea ice; Lewis, 1993) and by Pflug et al. (1993) that although the second order equation is adequate for many cases, a higher order is sometimes needed.

2.3. Generalized scale invariance in Fourier space

In geophysical applications, the scaling of the structure function:

$$S(\mathbf{x},\ \Delta\mathbf{x}) = \langle [u(\mathbf{x}) - u(\mathbf{x} + \Delta\mathbf{x})]^2 \rangle \tag{10}$$

of a field, $u(\mathbf{x})$, is often studied ($\mathbf{x}$ is a position vector, $\Delta\mathbf{x}$ is a lag with respect to $\mathbf{x}$ and "$\langle\ \rangle$" denotes an ensemble averaged quantity). If a scaling field is statistically homogeneous, then the structure function is independent of $\mathbf{x}$ and will scale as:

$$S(T_\lambda \Delta\mathbf{x}) = \lambda^{-\xi} S(\Delta\mathbf{x}), \tag{11}$$

where ξ is the scaling exponent and T_λ is the scale changing operator which relates the statistical properties at one scale to those at another. Note that we have eliminated the functional $\mathbf{x}$ dependence in the notation for S to highlight the statistical homogeneity. The solution to this functional equation is:

$$S(\Delta\mathbf{x}) \propto \|\Delta\mathbf{x}\|^{-\xi}. \tag{12}$$

Note that both anisotropic multifractals as well as anisotropic monofractals (such as anisotropic extensions of fractional Brownian motion) will generally obey Eq. (12). Since translations of structures change their Fourier phases but not moduli, for statistically homogeneous functions it is convenient to consider directly their moduli. The relevant scaling quantity is the spectral energy density (the Fourier transform of the auto-correlation function, or the second power of the Fourier amplitude of the field):

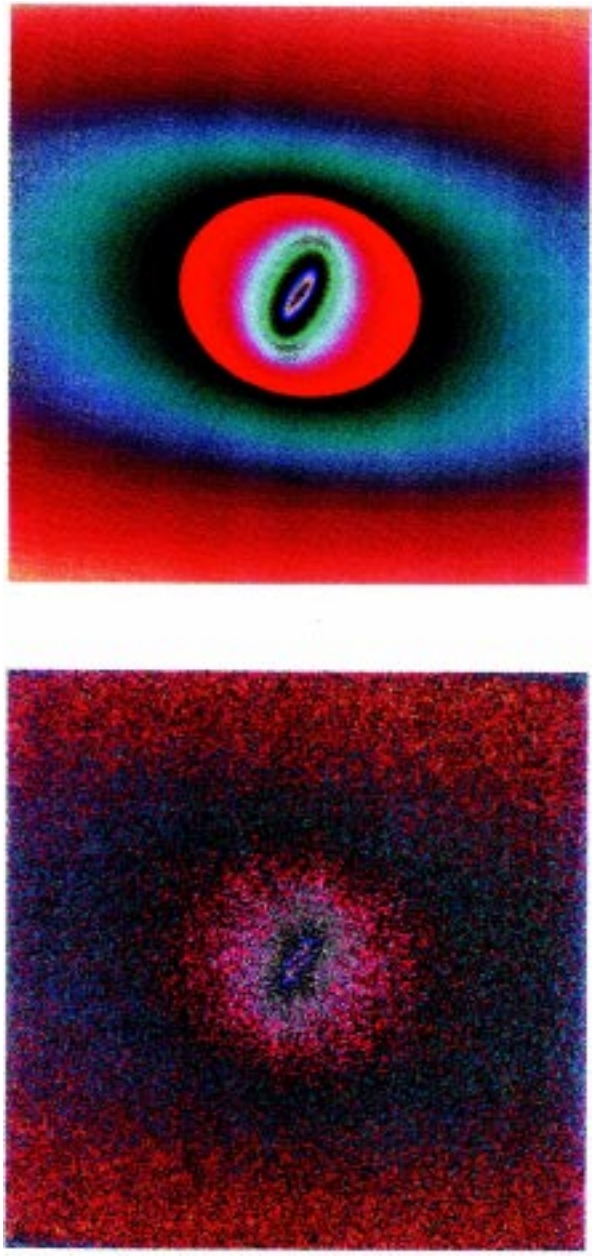

Fig. 2. Theoretical ensemble average spectral energy density (top) and corresponding single realization (multifractal simulation), bottom.

$$P(k) = |U(k)|^2 \tag{13}$$

where $U(\mathbf{k})$ is the Fourier transform of $u(\mathbf{x})$ and $\mathbf{k}$ is the wave number. Ensemble averaging $P(\mathbf{k})$ and integrating over all angles will give the energy spectrum, $E(k)$, see Section 1.

An anisotropic extension of Tauberian theorems for Fourier transforms of scaling functions (Schertzer and Lovejoy, 1991; Pflug et al., 1991) shows that if the structure function obeys Eqs. (11) and (12) then:

$$\langle P(\tilde{T}_\lambda k)\rangle = \lambda^{-s}\langle P(k)\rangle \tag{14}$$

where $\tilde{T}_\lambda = \lambda^{\tilde{G}}$ is the (dual) scale changing operator in Fourier space and $s = D_{el} - \xi$ is the anisotropic scaling exponent (D_{el} = Trace(G) is the "elliptical" dimension of the space). $\tilde{G}$ is the generator in Fourier space, and in the case of linear GSI, $\tilde{G} = G^T$, i.e. the transpose of the real space generator (Schertzer and Lovejoy, 1991; Pflug et al., 1991). This can be shown by using the integral definition of Fourier transform to find the operator in Fourier space which corresponds to the real space scale changing operator (shown through a simple change of variables). Note also the change in sign — a contraction in real space corresponds to a dilation in Fourier space, and vice versa. Once again, the general solution of the above is:

$$\langle P(\mathbf{k})\rangle \propto \|\mathbf{k}\|^{-s} \tag{15}$$

using the norm with respect to $\tilde{G}$. Since Eqs. (14) and (15) apply to Fourier space position vectors, $\mathbf{k}$, rather than the lag vectors, $\Delta\mathbf{x}$, the balls can be given a physical interpretation in terms of the energy density. Equation (15) shows that lines of constant $\langle P(\mathbf{k})\rangle$ are lines of constant $\|\mathbf{k}\|$ (which are lines of constant scale); hence they can be identified with the frontiers of the balls, and $\tilde{T}_\lambda$ will map any contour to all the others. For convenience, since for the remainder of the paper we will only be considering scaling in Fourier space, the tilde will be dropped with the understanding that we are referring to the Fourier space generator.

3. The scale invariant generator technique

The purpose of this technique is to quantify scaling anisotropy by determining the parameters of the scale invariant generator and the balls that best describe a scaling field. Note that the scaling will not hold exactly on any individual realization, but only when averaged over an ensemble of realizations with the same generator and family of balls; there will be random variability about the ensemble mean $\langle P(\mathbf{k})\rangle$. Fig. 2 shows the spectral energy density of a simulated single realization (bottom) and its ensemble average counterpart (top). Also, the anisotropy will change from place to place and from time to time, thus G itself presumably varies stochastically from realization to realization (e.g. scene to scene, for satellite imagery). An attempt to empirically estimate the ensemble average by averaging many arbitrary realizations would therefore result in a smearing of the parameters (since each realization would have a different generator). Therefore, only one realization will be analyzed at a time and fluctuations about the ensemble average contours of the spectral energy density will be compensated for by using statistical regression techniques.

The nonlinear statistical regression involves fitting the theoretical function, $P_t(\mathbf{k})$ (the ensemble average spectral energy density generated from the GSI parameters) to the N data points, $P(\mathbf{k}_i)$, (the spectral energy density of the real space data known at the N discrete wave numbers, $\mathbf{k}_i$). Here, $P_t(\mathbf{k}) = \lambda^{-s}\langle P_1\rangle$, where $\langle P_1\rangle$ is the value of the spectral energy density at ∂B_1 and $\lambda = \|\mathbf{k}\|$ depends on G and B_1 (that is, the scale of a certain point, $\mathbf{k}$, will be different for different G and B_1). Usual statistical procedures involve the method of least-squares, where the parameter estimates are determined by minimizing an error function E^2 (not to be mistaken with the energy spectrum E(k), see ++Section 2.3) which we take here as:

$$E^2(G, B_1, \langle P_1\rangle, s) = \frac{1}{N}\sum_{i=1}^{N}[\ln P(\mathbf{k}_i) - \ln P_t(\mathbf{k}_i,\ G,\ B_1,\ \langle P_1\rangle,\ s)]^2, \tag{16}$$

where the full functional dependence of P_t has been included. Other error functions may be defined, but we chose the above based on the difference of logarithms (see discussion below). Note that, from Eq. (14), $\ln P_t = -s\ln\lambda + \ln\langle P_1\rangle$, where the scale ratio, λ, corresponding to each $\mathbf{k}_i$ must be found by solving a transcendental equation (involving G and B_1).

G is a function of c, f and e (since by convention $d = 1$) and B_1 is a function of the unit ball parameters (see, for example, Eq. (9)). The parameter space is therefore at least eight-dimensional (the exact dimension depends on the parametrization of B_1). Searching for the absolute minimum of E^2 in such a large parameter space is computationally prohibitive, even when a transcendental equation need not be solved. Therefore, it is necessary to make some approximation to the error function of Eq. (16). The Monte Carlo differential rotation method (Pflug et al., 1993) attempted to do this by estimating the ball parameters before searching the parameter space of $G(c, f, e)$. However, this is not an ideal solution since the statistical scatter of P led to errors in the estimates of B_1, which introduced biases in the estimates of G.

The scale invariant generator technique (SIG) has the significant advantage of being able to estimate the more fundamental G without prior knowledge of B_1. It reduces the parameter space to four dimensions (c, f, e, s) without introducing errors due to the prior estimation of other parameters. If the anisotropy is not extreme, it is possible to obtain a good prior estimate

for s from the isotropic energy spectrum ($s=\beta+1$; see Pflug et al., 1991) and thus reduce the dimension of the parameter space further. This method was used in the analysis below, however, in general, the full four-dimensional parameter space can be considered.

To see how SIG eliminates any reference to B_1, denote by $\mathbf{k}_1(\theta)$ a vector on ∂B_1 parametrized by θ (the polar angle is convenient). Then we can parametrize all vectors, $\mathbf{k}$, using λ_1 and θ instead of the usual Cartesian coordinates. This can be seen by writing $\mathbf{k}(\lambda_1,\theta) = T_{\lambda_1} k_1(\theta)$ and noting that all $\mathbf{k}$ lie on one and only one trajectory which originates from a single point on ∂B_1 (θ parametrizes the trajectory and λ_1 the points along the trajectory). Further dilations by a factor λ_2 (i.e. $\mathbf{k}(\lambda_2\lambda_1,\theta) = T_{\lambda_2}\mathbf{k}(\lambda_1,\theta) = \lambda_2^G \mathbf{k}(\lambda_1,\theta)$) obey:

$$\langle P(\lambda_2^G \mathbf{k}(\lambda_1,\theta))\rangle = \lambda_2^{-s}\langle P(\mathbf{k}(\lambda_1,\theta))\rangle \tag{17}$$

(from Eq. (14)). Since λ_2 and $\mathbf{k}(\lambda_1,\ \theta)$ are arbitrary, this equation shows (with taking logarithms) that for *all* λ and $\mathbf{k}$

$$\ln\langle P(\lambda^G \mathbf{k})\rangle + s\ln\lambda - \ln\langle P(\mathbf{k})\rangle = 0 \tag{18}$$

must be satisfied, i.e. all pairs of points along trajectories will (on average) satisfy Eq. (18). The basic approximation we make is simply to replace ensemble averages by averages over trajectories. That is, we find G such that the quantity in Eq. (18) averaged over trajectories is as close to zero as possible. The scale invariant generator (SIG) error function used in the analysis is defined as:

$$E^2_{\mathrm{SIG}}(G,\ s) = \frac{1}{n}\sum_{i,j}[\ln P(\lambda_i^G \mathbf{k}_j) + s\ln\lambda_i - \ln P(\mathbf{k}_j)]^2. \tag{19}$$

The sum is over all the data points, $P(\mathbf{k}_j)$, and all the possible (discrete) scale ratios, λ_i , which form the n unique pairs $[P(\lambda_i^G \mathbf{k}_j),\ P(\mathbf{k}_j)]$, i.e. E^2_{SIG} compares all possible pairs of data points which lie along common trajectories. The power of the SIG error function can be seen in two ways. First, since there is no reference to the unit ball in Eq. (19), no information concerning it is necessary to compute G. Second, since it is expected that we will not need all the pairs to obtain adequate statistics, we can simply choose λ_i and $\mathbf{k}_j$, from which $\lambda_i^G \mathbf{k}_j$ can be easily computed, and thus a transcendental equation need not be solved. For simplicity, we will now refer to E^2_{SIG} (Eq. (19)) as E^2.

Since it is not possible to analytically solve for the minimum of E^2, it is necessary to consider E^2 as a continuous function of the four parameters that describes a four-dimensional hypersurface. The parameter space must be searched for the appropriate minimum (i.e. E^2 must be found numerically at intervals in parameter space to trace out the behavior of the hypersurface). In general, E^2 can be a complicated function with multiple extrema. Therefore, if the absolute minimum is to be found, the intervals must be fine enough such that the estimate of the hypersurface exhibits the same extrema. The hypersurface, however, is expected to be continuous only when an infinite number of independent pairs is used. Since this would require knowledge of P over an infinite range of scales, the actual explicit values of E^2 are expected to be statistically scattered around the theoretical continuous hypersurface. Due to these high frequency fluctuations, a function is fit to the explicit values of E^2 in an attempt to estimate the continuous hypersurface. The estimated minimum of E^2 can then be found by calculating the minimum of the fitted function.

It is important to note that $P(\lambda_i^G \mathbf{k}_j)$ and $P(\mathbf{k}_j)$ are data points (i.e. random variables) and therefore both will fluctuate about their average values. This will cause the minimum variance (the minimum value of E^2) to be larger than the case when only one data point is involved. However, it should be possible to compensate for this by use of the greater number of pairs that is available. There is a complication in that the fluctuations of the data points will be more variable than those described by multivariate Gaussian distributions. Therefore, there is no rigorous theoretical justification for using the method of least-squares. However, it is still plausible to assume that the behavior of the hypersurface near the minimum will not be substantially altered if the fluctuations are not too violent. Logarithms of P were used in E^2 since numerical tests showed that taking the logarithm has the effect of decreasing the variability. The results shown below justify the use of the method of least squares and indicate that the bias due to taking the logarithm was small.

4. Implementation

Finding the absolute minimum of E^2 will give the generator parameter estimates. In order for the technique to be practical, it must find the minimum with reasonable accuracy in an efficient manner. There are many standard methods of searching a parameter space for the minimum of hypersurfaces such as E^2. The most appropriate method, however, depends on the nature of the hypersurface and the statistical fluctuations about it. Therefore, the characteristics of E^2 were studied. It was found that performing an initial estimate using coarse intervals covering the parameter space, followed by a (multidimensional) parabolic expansion about the initial estimate, was necessary. Although it is less expedient than methods that only require iterations of a one-dimensional search, it is more reliable. For more details see Lewis (1993).

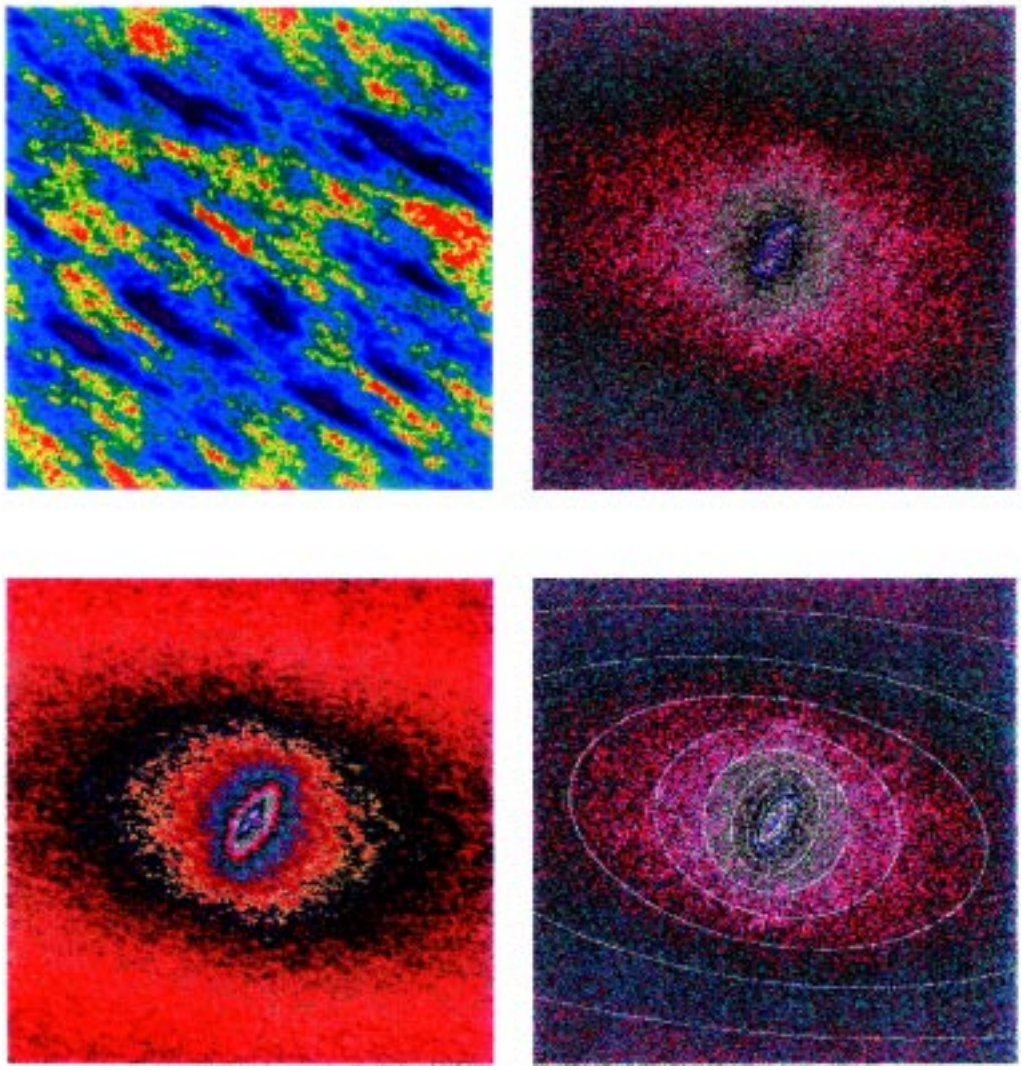

Fig. 3. Simulation 1. Top left: in real space. Top right: spectral energy density. Bottom left: enhanced spectral energy density. Bottom right: spectral energy density with estimated balls. See Table 1 for results.

Before implementation, it is necessary to consider the following details:

1. The number and distribution of pairs. The error function, E^2, compares all pairs of points along a trajectory. This would mean comparing approximately $(L^3)/4$ pairs, where there are L^2 data points. It is expected that not all pairs need be considered in order to obtain a reasonable estimate of the corresponding value of the continuous hypersurface. Not only will this lead to faster computation, it will also eliminate the difficulty of finding all the pairs. Also, due to undersampling at the large wave numbers and the possible biases at the small wave numbers that are sometimes introduced in the data acquisition, it is prudent to choose the pairs such that the large and small wave numbers are not oversampled. Thus, the adequate number of pairs, and a method of choosing the pairs, must be found.
2. The spacing of points in parameter space which is needed for a reasonable estimate of the continuous hypersurface. If the spacing is too coarse, important details of the hypersurface may be missed, but since computation time increases with resolution, it may be counter-productive to have the spacing too fine.
3. The optimum range of the parabolic expansion. Since the hypersurface is not parabolic, the range should correspond to a neighborhood of the minimum where the hypersurface can be well approximated by a parabola. However, if the range is too small, it is possible that the curvature would not be

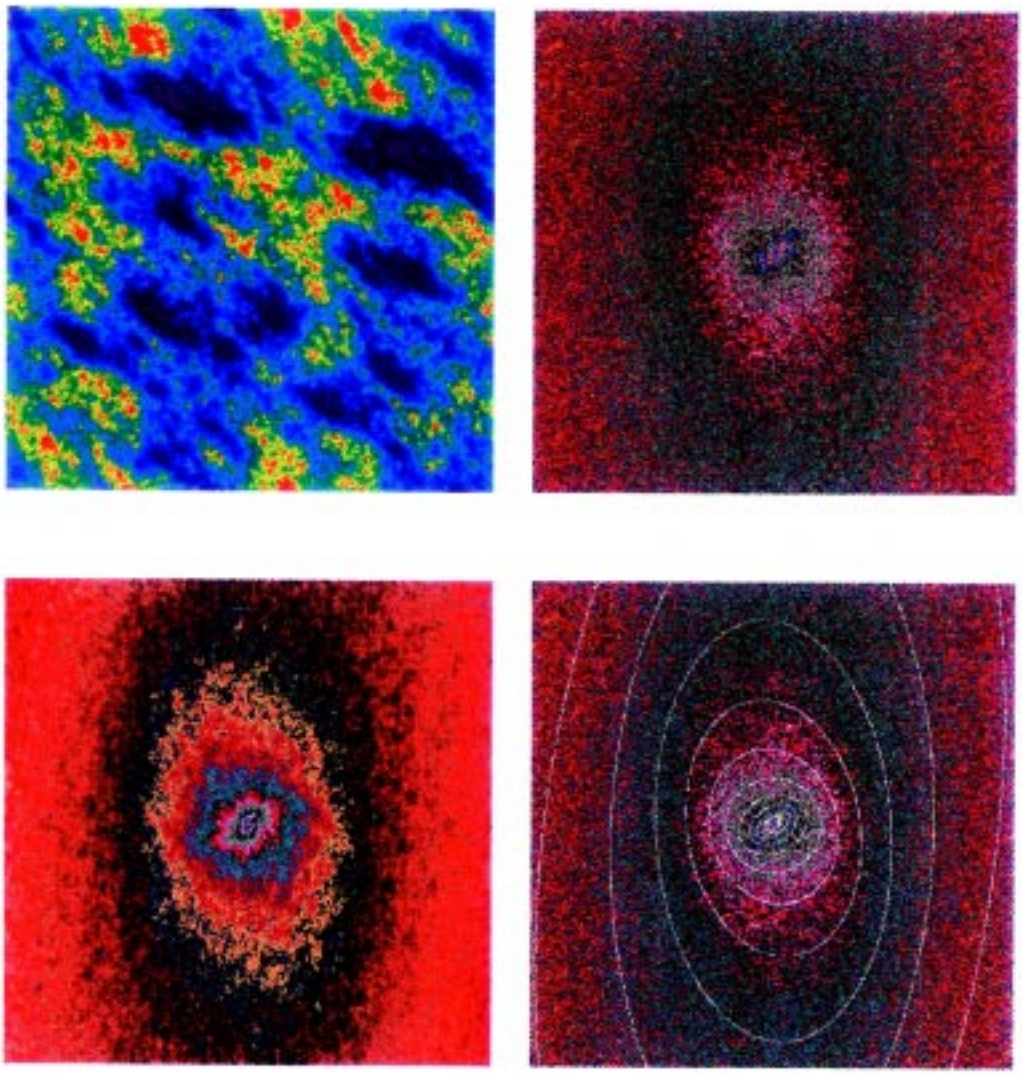

Fig. 4. Simulation 2. Top left: in real space. Top right: spectral energy density. Bottom left: enhanced spectral energy density. Bottom right: spectral energy density with estimated balls. See Table 1 for results.

detectable over the fluctuations. If the range is too great, the higher order terms in the expansion of the hypersurface become non-negligible and errors are introduced.

4. The volume of the initial search. Before the initial search, it would be beneficial to find the region in parameter space which leads to valid GSI systems (imposed by the non-crossing condition of the balls). Searching outside this region would be a waste of computation time.

In order to make intelligent choices for Eqs. (1)–(4), each was investigated through various methods and numerical experiments. The actual choices that were made may not be of general interest. Therefore, should readers wish more details, they are referred to Lewis (1993 ++Section 3.2.2), which contains a thorough explanation of methods and choices, with examples and results. We should note, however, that our philosophy was to make choices such that the errors in the estimates were within a range that we judged to be reasonable. If the errors were too large, the estimates were considered inaccurate and if they were too small, it was considered to be a waste of computing time, since small changes in the parameters cause no observable morphological difference in the fields.

5. Estimation of the balls

The next step is the estimation of the family of balls.

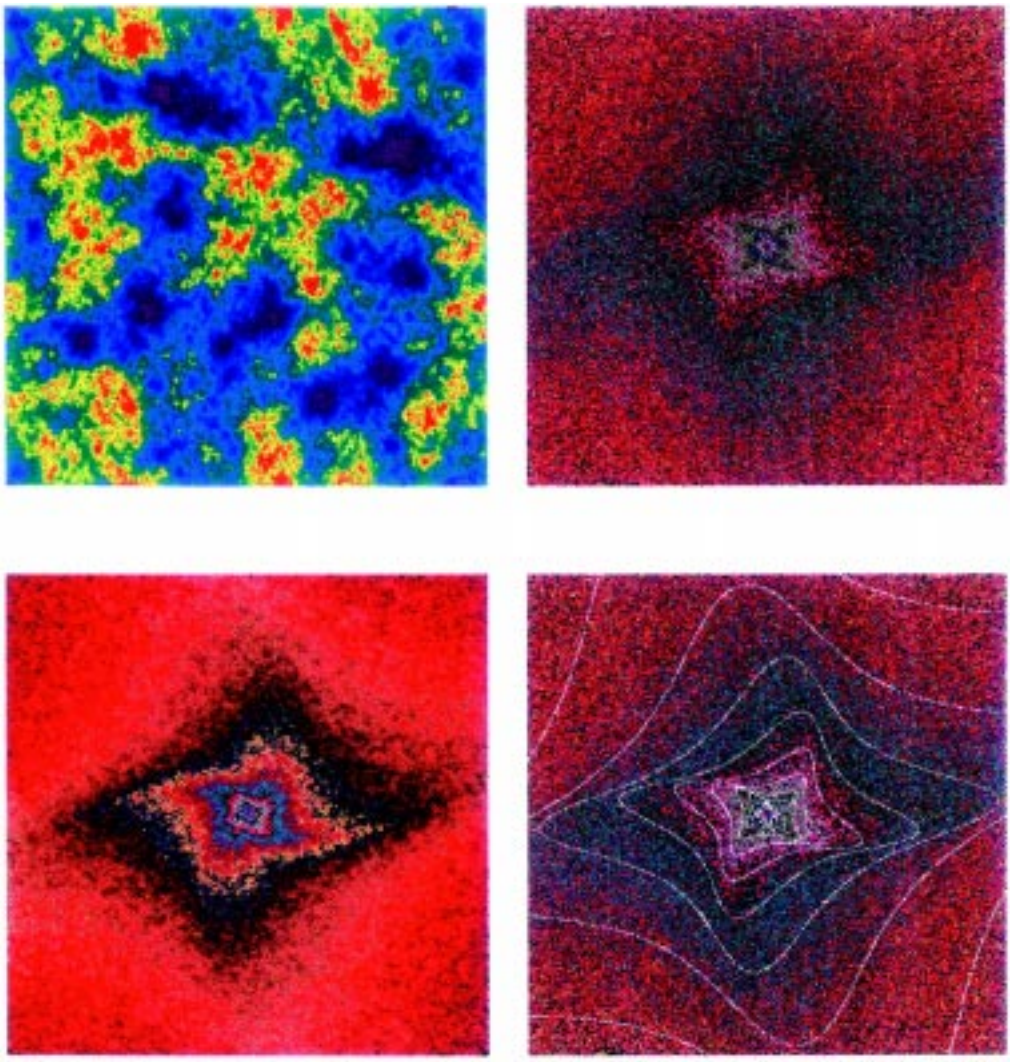

Fig. 5. Simulation 3. Top left: in real space. Top right: spectral energy density. Bottom left: enhanced spectral energy density. Bottom right: spectral energy density with estimated balls. See Table 1 for results.

Once any one member of the family of balls is found, the whole family can be generated, since the generator has already been estimated. Thus, the estimation consists of finding the parameters that describe some ball, which will be approximated by a second or fourth order polynomial (see Section 2.2).

Unlike the generator parameters, an analytic method may be used to estimate the ball parameters. These estimates may be found by fitting a curve of the appropriate form to a levelset of the spectral energy density (where a levelset at P_1 is the set of data points with amplitude in the range $P_1 \pm \Delta P$, ΔP small). See Lewis (1993) for the method of curve fitting and method of determining the appropriate form of the curve. Because the large fluctuations about the ensemble average contours cause undesirable errors in the parameter estimates, ideally, the spectral energy density, P, could be smoothed before the fitting procedure. Conventional smoothing (e.g. averaging adjacent data points) causes non-uniform spreading of the contours of P and consequently, the smoothed field will not be described by the same GSI parameters as the actual P.

Assuming that the estimates of the generator parameters, found using the SIG error function of Eq. (19), are reasonably accurate, they can be used to "enhance" the contours of P without affecting the scaling of the field. Regardless of this assumption, fitting a curve to a levelset of the enhanced P will find the best estimate of a unit ball given the estimated generator parameters.

Table 1
Estimated parameters with standard deviations (square root of uncertainites) for simulations. Simulations 1 and 2 have sphero-scale and thus all balls are quadratic. Sphero-scales are given in units^{-1}, where external scale is defined to be at one unit. Sphero-scale can be found from estimated ball if quadratics are used and sphero-scale exists (see Lewis, 1993). Note that errors were not calculated on sphero-scale measurements since errors that were found on ball parameters (~1%, from mean-squared deviation from contour of ensemble average P) are magnified non-trivially with scale transformation. For simulation 3, estimated ball is given by $2.58k_x^4+21.74k_x^3k_y+9.46k_x^2k_y^2-11.38k_xk_y^3+9.76k_y^4=10^{-3}$ and error is also ~1%

Simulation	Parameters	s	c	f	e	Sphero-scale
1	exact	2.64	0.3	0.2	0.3	0.146
	estimated	2.69 ± 0.04	0.28 ± 0.01	0.20 ± 0.01	0.31 ± 0.03	0.149
2	exact	2.64	−0.2	0.2	−0.6	0.098
	estimated	2.53 ± 0.04	-0.19 ± 0.01	0.18 ± 0.01	-0.54 ± 0.06	0.100
3	exact	2.64	0.1	0.1	0.5	N/A
	estimated	2.63 ± 0.03	0.05 ± 0.01	0.08 ± 0.01	0.51 ± 0.01	N/A

The enhancing technique consists of applying a running average to the data points that lie on the same trajectory. Again we will use the principle that the amplitude of any two data points on the same trajectory (specified by θ) will be, on average, related by:

$$\langle P(\lambda^G \mathbf{k}(\theta)\rangle = \lambda^{-s}\langle P(\mathbf{k}(\theta))\rangle. \tag{20}$$

As before, an approximation is made such that only M data points are used in the running average. That is, to generate the enhanced P, $P_{en}(\mathbf{k}_j)$, the amplitude of each data point, $P(\mathbf{k}_j)$, is replaced by

$$P_{en}(\mathbf{k}_j) = \frac{1}{M}\sum_{i=1}^{M}\lambda_i^s P(\lambda_i^G \mathbf{k}_j) \tag{21}$$

where λ_i are a series of dilation factors. It can be seen from the results that the enhancing technique has a substantial smoothing effect. See bottom left of Figs. 3, 4 and 5.

The parameters of a unit ball, B_1 at some chosen P_1, were found by fitting the appropriate polynomial to a levelset of $P_{en}(\mathbf{k}_j)$. Recently, an extension for finding the balls has been developed. This new procedure has the advantage that it is global (not restricted to one levelset). It is therefore more accurate. However, it is not as fast as the procedure used here and the increased accuracy has not been deemed necessary for the present purposes.

6. Results on simulations

The scale invariant generator technique was tested using simulations of continuous multiplicative cascades which yield universal multifractals (Schertzer and Lovejoy, 1987; Wilson et al., 1991; Pecknold et al., 1993). Multifractal fields were chosen as the test fields because we feel that they are the most relevant in geophysics and also, due to the extreme variability of multifractals, they will, in fact, be more challenging to analyze than other anisotropic scale invariant fields (e.g. monofractals, such as fractional Brownian motion or anisotropic monofractals produced by the fractal sum of pulses model (Lovejoy and Schertzer, 1985)). It should be noted that the scale invariant generator technique is not restricted to multifractals and can be used, without modification, to analyze the spectral energy density of any scaling field (or, using indicator functions, anisotropic fractal sets), regardless of the type of scaling expected, as long as statistical translational invariance of the underlying generation process is assumed.

The basic steps in the simulation of universal multifractals are: (a) the production of a "δ−correlated" (extremal) Lévy noise, the "sub-generator", that determines the type of probability distribution (parametrized by α and C_1), (b) anisotropic filtering to produce an (anisotropic) $1/f$ noise, the multifractal generator, (c) exponentiation to produce the conserved multifractal, (d) a final (anisotropic) fractional integration (differentiation), of order H (positive H implies a scale invariant fractional integration). For details of the method used to render the filtering algorithm anisotropic, see Pecknold et al. (1993). For multifractal fields, the probability that ε_λ, at resolution λ, will exceed λ^γ is:

$$\Pr(\varepsilon_\lambda \gamma \geq \lambda^\gamma) \approx \lambda^{-c(\gamma)}, \tag{22}$$

where $c(\gamma)$ is the codimension which is some function of $\gamma \equiv$ the order of singularity (Schertzer and Lovejoy, 1987). Therefore, in general, there will be a unique value of c for each γ, thus an infinite hierarchy of fractal dimensions corresponding to all $\gamma \in \mathscr{R}$. Scaling fields with this property are multifractals and they are characterized by their extreme variability (Schertzer and Lovejoy, 1987). In the case of a universal multifractal, the three parameters α, C_1, and H determine

$c(\gamma)$: $\alpha(0 \leq \alpha \leq 2)$ is a measure of the degree of multifractality ($\alpha=0$: monofractal, $\alpha=2$: log normal multifractal), C_1 is a measure of the sparseness of the mean of the field and H is a measure of the degree of non-conservation of the field (see Schertzer and Lovejoy, 1991).

A variety of different generator and ball parameters were tested using SIG, while the multifractal parameters were held constant at: $\alpha=1.5$, $C_1=0.1$, $H = 0.4$. These values are close to those found empirically in cloud radiances (Tessier et al., 1993) and turbulent winds and temperatures (Schmitt et al., 1992; Schmitt et al., 1995; Schmitt et al., 1996). The effects on the accuracy of the technique due to changes in these parameters are studied below. The simulations considered were 512×512 pixels in size (which is a typical size of many geophysical data sets/satellite images). The simulations were all generated from the same random sub-generator so that the changes in the characteristics of the fields due to the different GSI parameters could be seen more clearly. The spectral energy density, P, was found by using a fast Fourier transform technique (Press et al., 1986).

The results of each simulation are presented in Figs. 3, 4 and 5 and Table 1 (for further results see Lewis, 1993). The accuracy of the estimated parameters can be seen quite well in the images where the balls generated by the estimated parameters are drawn over the spectral energy density and also by comparison with the enhanced P. A discussion of the results and the accuracy of the estimated uncertainties is given in ++Section 7.

Note that if the estimated ball parameters are accurate, they should describe a contour of constant P. Thus, the accuracy of the fit can be determined by observing if the value of an ensemble average P, with the theoretical generator and ball parameters, is constant along the estimated ball. The mean-squared deviation from the constant value of P can be used as a measure of the goodness of the fit. The percentage deviations from the constant were found to be very close to 1% in all cases.

7. Discussion of results and investigation of the accuracy of the uncertainties

From the results on the simulations above, it can be seen subjectively that, the estimated balls, drawn over P, seem to reasonably match the contours of P. However, in many cases, the discrepancies between the estimated and theoretical parameter values are somewhat larger than what would be expected from the estimated standard deviations. A closer investigation is necessary because it is not known if the discrepancies are due to an underestimation of the uncertainties (higher statistical fluctuations than assumed) or if they are an indication of biased parameter estimates. Thus, it is necessary to investigate the accuracy of the estimated uncertainties.

Table 2
Parameter estimates and standard deviations for 10 different realizations (with GSI parameters: $c = 0.3$, $f = 0.2$, $e = 0.3$) found using SIG

Simulation	c	σ_c	f	σ_f	e	σ_e
1	0.319	0.010	0.168	0.009	0.395	0.025
2	0.306	0.010	0.166	0.009	0.328	0.023
3	0.297	0.010	0.203	0.009	0.300	0.023
4	0.316	0.010	0.214	0.009	0.379	0.024
5	0.324	0.010	0.183	0.009	0.366	0.022
6	0.329	0.010	0.199	0.009	0.305	0.025
7	0.295	0.011	0.167	0.009	0.292	0.026
8	0.342	0.010	0.183	0.009	0.489	0.023
9	0.322	0.011	0.183	0.009	0.288	0.026
10	0.292	0.012	0.192	0.009	0.331	0.027

Since the minimum of E^2 could not be found analytically, neither could the uncertainties. However, they can be estimated by making an analogy to the case when an analytic solution is possible (i.e. the case when parabolic expansion describes the hypersurface exactly). The estimated uncertainties on the GSI parameters will then be

$$\sigma_{g_k}^2 = \frac{\epsilon_{kk} E_{\min}^2}{n} \tag{23}$$

where g_k ($k = 1, 2, 3$) are (c, f, e) respectively, ϵ_{kk} are the diagonal elements of the error matrix $\epsilon=\alpha^{-1}$, $\alpha_{ij}=(1/2)(\partial^2 E^2/\partial g_i \partial g_j)$ (evaluated at the minimum), n is the number of pairs of data points compared (as in E^2) and $E_{\min}^2$ is the value of E^2 at its minimum.

The estimated uncertainties, $\sigma_{g_k}^2$, are expected to be reasonable estimates of the actual uncertainties if the n pairs of data points compared are effectively independent, if the hypersurface can be reasonably approximated by a parabola and if the statistics are approximately Gaussian. These ideal conditions, however, will not be met and it is unknown exactly how the deviations from the ideal will effect the accuracy of the $\sigma_{g_k}^2$. It is possible to check the accuracy by using the fact that $\sigma_{g_k}^2$ is an estimate of the realization to realization variability in the parameter estimates due to the statistical fluctuations of the data. That is, if an ensemble of realizations are analyzed, then the actual uncertainties are the variances of the parameter estimates about their respective mean values. Therefore, in order to obtain a direct estimate of the actual uncertainties, the analysis was performed on ten different simulations that were created with the same GSI and multifractal parameters but with different random sub-

Table 3
Standard deviations, ς_{g_k}, calculated from variance of estimates of parameters (listed in Table 2) about $\bar{g}_k$ (listed in Table 4) and typical estimated standard deviations, σ_{g_k}, expected from Eq. (23) (as in Table 2)

g_k	c	f	e
ς_{g_k}	0.015	0.016	0.059
σ_{g_k}	0.010	0.009	0.024

generators. Results are shown in Table 2. The standard deviations, ζ_{g_k}, were calculated from the sample variances, $\zeta^2_{g_k}$, of the parameter estimates of the ten realizations about their mean values, $\bar{g}_k$. ζ_{g_k} are listed in Table 3 along with typical values of the estimated σ_{g_k} for comparison. $\bar{g}_k$ are listed in Table 4 with the actual simulation parameter values. See top left of Fig. 3 for one example of a realization. The actual parameter values used are similar to those found for cloud radiance fields for stratus type clouds.

We see that the σ_{g_k} are underestimates of the realization to realization standard deviations, ζ_{g_k}. However, they are within about a factor of two. If we assume that all the uncertainties listed in ++Section 6 are underestimated by a similar magnitude, we can conclude that the bias in the GSI parameter estimates is small (even though it cannot be altogether ruled out). Below, the uncertainties calculated using Eq. (23) will be used as the estimated uncertainties with the understanding that they are underestimates. Because the results of this section will depend on the multifractal parameters (statistical properties of the field), in general, they cannot be used to improve the estimates of the uncertainties.

Another point of interest is the discrepancies between the mean values of the estimates, $\bar{g}_k$, and the theoretical values of the parameters. These discrepancies could be an indication of bias since the standard deviation in $\bar{g}_k$ is:

$$\frac{1}{\sqrt{10}}\varsigma_{g_k} \tag{24}$$

i.e. $\bar{g}_k$ do not lie within one standard deviation of their theoretical values. Note, however, that the bias is still somewhat small ($\sim$0.01 for c and f; $\sim$0.03 for e; two ensemble average P differing by this amount will be virtually indistinguishable). Although this bias tends to overestimate c and e, and underestimate f, there seems to be no evidence of a systematic overestimation (or underestimation) of the parameters in ++Section 6. This implies that the bias may be different for each generator. Some bias could be due to the non-parabolic characteristic of the hypersurface. This bias could then be reduced by decreasing the range of the parabolic expansion. Because this is expected to increase the realization to realization variability, it is unclear if the change would yield better estimates.

We can therefore conclude that SIG yields reasonable results and thus the use of a least-squares method based on the difference of logarithms is supported even though it is not theoretically justifiable.

Table 4
Mean values, $\bar{g}_k$, of estimates of parameters of ten realizations listed in Table 2 and actual simulation values

g_k	c	f	e
Mean values	0.314	0.186	0.347
Actual values	0.3	0.2	0.3

8. The effects of the multifractal parameters on the GSI parameter estimates and their corresponding uncertainties

We will now investigate the accuracy with which the SIG technique measures the GSI parameters of fields with different statistical properties (e.g. different anisotropic scaling exponents and noise characteristics). For universal multifractals, these properties are described by the multifractal parameters: α, C_1 and H (see e.g. Schertzer and Lovejoy (1991) for a comparison of the estimated multifractal parameters of various geophysical fields see Lovejoy and Schertzer (1995)).

It is expected that the anisotropic scaling exponent, s, will be a major determinant of the accuracy since it determines the rate of decay of the amplitude of the spectral energy density, P, with scale. As s decreases, the contours of P become less distinguishable: we expect some s at which the technique will no longer yield reasonable estimates. Equivalently, the curvature of the hypersurface will decrease with decreasing s and thus, the uncertainties in the GSI parameter estimates will increase.

For universal multifractals, the exponent, s, is determined in the following manner:

$$s = 2 - \frac{C_1}{\alpha - 1}(2^{\alpha} - 2) + 2H \tag{25}$$

(see e.g. Tessier et al., 1993). Thus, the uncertainties will predominately depend on C_1 and H. H is expected to effect the results solely in its contribution to s, however, C_1 is a direct measure of the amplitude of the noise (i.e. the contours will be less distinguishable due to an increase in C_1). The weak dependence of the uncertainties on α will not be studied.

The SIG technique described was used to analyze 10 simulations ($c = 0.3$, $f = 0.2$, $e = 0.3$) with different

Table 5
Dependence on C_1 of parameter estimates and standard deviations of universal multifractal simulations found using SIG. H = constant = 0.4

C_1	s	c	σ_c	f	σ_f	e	σ_e
0.05	2.78	0.293	0.011	0.186	0.009	0.383	0.025
0.10	2.69	0.293	0.012	0.190	0.009	0.334	0.028
0.15	2.61	0.302	0.013	0.199	0.009	0.319	0.029
0.20	2.53	0.272	0.015	0.208	0.010	0.279	0.035
0.25	2.45	0.275	0.015	0.216	0.010	0.291	0.033
0.30	2.38	0.256	0.018	0.210	0.010	0.269	0.036
0.35	2.30	0.295	0.019	0.218	0.011	0.312	0.034
0.40	2.23	0.304	0.021	0.232	0.011	0.307	0.037
0.45	2.16	0.340	0.021	0.231	0.012	0.346	0.033
0.50	2.10	0.274	0.026	0.227	0.012	0.262	0.039

values of C_1 (see Table 5). H and α were held constant at 0.4 and 1.5, respectively. The uncertainties were then studied as a function of H (for constant $C_1 = 0.1$; $\alpha = 1.5$). See Table 6. It was found that the technique was only able to obtain valid results for $H \geq -0.1$ ($s \geq 1.59$). Below this value of H, small decreases in H resulted in a large increase in the uncertainties. The curvature of the hypersurface presumably became negligible compared to the fluctuations about the hypersurface.

Although valid results were obtained for all values of C_1 that were studied, it is expected there will also be a critical C_1 above which the uncertainties will increase quickly. There will also be a combination of effects due to C_1 and H. This, however, was not studied further.

The above results indicate that SIG can yield valid estimates for a range of multifractal parameters that is adequate to include a large variety of geophysical fields. However, simple changes such as increasing the number of points considered or changing the range of parabolic expansion can extend the range of validity. For example, by changing the range of the parabolic expansion, valid results were obtainable for $H \geq -0.3$.

Table 6
Dependence on H of parameter estimates and standard deviations of universal multifractal simulations found using SIG. C_1 = constant = 0.1

H	s	c	σ_c	f	σ_f	e	σ_e
0.4	2.69	0.293	0.012	0.190	0.009	0.334	0.028
0.3	2.49	0.292	0.014	0.191	0.010	0.332	0.029
0.2	2.25	0.302	0.015	0.186	0.011	0.345	0.033
0.1	2.02	0.282	0.018	0.194	0.013	0.299	0.039
0.0	1.80	0.286	0.022	0.198	0.015	0.283	0.045
−0.1	1.59	0.270	0.038	0.188	0.023	0.278	0.084

Table 7
Dependence on H of parameter estimates and standard deviations of universal multifractal simulations found using SIG with extended range of parabolic approximation (C_1 = constant = 0.1)

H	s	c	σ_c	f	σ_f	e	σ_e
−0.2	1.38	0.274	0.02	0.132	0.02	0.294	0.05
−0.3	1.16	0.266	0.02	0.129	0.02	0.220	0.05

See Table 7. Note the discrepancies of the estimated parameters from the theoretical (simulation) parameters are much greater for this case. This is likely due to the increased range of expansion coupled with the non-parabolic nature of the hypersurface.

Finally, it should be noted that the above results were obtained for a given set of GSI parameters and would be expected to change slightly depending on them. However, the overall observations are not expected to change.

9. Conclusion

In this paper, the scale invariant generator technique (SIG) was developed to estimate the parameters of a linear generalized scale invariant system. It is able to estimate the generator parameters without prior knowledge of the GSI balls. This is an advantage over the previous method (the Monte-Carlo differential rotation technique). It then uses the estimated generator parameters to enhance the spectral energy density and thus it was able to produce good estimates of the GSI balls. Universal multifractal simulations, generated with a variety of GSI and multifractal parameters, were used to test the technique. It was found that SIG reasonably estimated the GSI parameters for a variety of anisotropy as well as over a large range of multifractal parameters. Specifically, virtually all of the geophysical fields whose multifractal parameters are known have parameters which allow them to be analyzed by SIG. Thus, it can be concluded that SIG could plausibly be used to quantify the anisotropy of many geophysical fields.

It was stated that the GSI parameters may be used as a measure of texture and morphology. While this was not tested here, by inspection of the simulated images, it can be seen that the different GSI parameters correspond to different characteristics of the fields. For example, when applied to satellite cloud radiances (Pecknold et al., 1997b), it yields a scale invariant cloud classification. Although cases involving overall stratification (such as time/space or vertical/horizontal cross-sections) were not explicitly discussed, they are also found (work in progress) to be amenable

to SIG analysis (although s can not be estimated using the isotropic approximation). Such space-time analyses (Tessier et al., 1993; Marsan et al., 1996) are important for dynamical multifractal modeling and forecasting (Marsan et al., 1996).

Now that a numerically efficient procedure exists for estimating GSI parameters, future research should include the application of SIG to a large number of scenes of a variety of geophysical fields. This is not only necessary for the possible application to classification mentioned above, but this will also allow the statistical properties of the generator to be studied. In addition, the full nonlinear GSI, rather than the linearization assumed here, could be applied. Also, a real space version of SIG is being developed which will make it possible to find the generator for different order statistics since they will not necessarily have the same anisotropy as the second order statistics discussed here. This would be necessary if the full potential of GSI and the scale invariant generator technique is to be realized.

Acknowledgements

The authors would like to thank J.F. Malouin and C. Hooge.

Appendix A. The scale uniqueness condition for the case of quadratic balls

Given that the GSI balls are described by the quadratic Eq. (9), we can derive a general scale uniqueness condition. Defining $\mathbf{A}_\lambda$ by $f_\lambda(\mathbf{x}) = \mathbf{x}^T\mathbf{A}_\lambda\mathbf{x}$, we have:

$$\mathbf{A}_\lambda = (T_\lambda^{-1})^T\mathbf{A}_1 T_\lambda^{-1} = \lambda^{\boldsymbol{G}^T}\mathbf{A}_1\lambda^{\boldsymbol{G}}. \tag{A.1}$$

The scale uniqueness condition (Eq. (5)) reduces to:

$$\mathbf{x}^T \operatorname{sym}(\mathbf{A}_\lambda \boldsymbol{G})\boldsymbol{x} > 0, \tag{A.2}$$

where $\operatorname{sym}(\mathbf{A}_\lambda \boldsymbol{G}) = ((\mathbf{A}_\lambda \boldsymbol{G} + \boldsymbol{G}\mathrm{A}_\lambda)/2)$. Condition (A.2) is satisfied for all $\mathbf{x}$ as long as the eigenvalues of $\operatorname{sym}(\mathbf{A}_\lambda \boldsymbol{G})$ are positive (in two dimensions this is the same as requiring both the trace and determinant to be positive). To obtain the noncrossing condition in the general quadratic case one can write:

$$\operatorname{sym}(\mathbf{A}_\lambda \boldsymbol{G}) = D\mathbf{1} + F\mathbf{J} + C\mathbf{K}, \tag{A.3}$$

where $\mathbf{1}$, $\mathbf{J}$ and $\mathbf{K}$ are as in Eq. (7) and D, F and C are real numbers. Since $\operatorname{Trace}(\operatorname{sym}(\mathbf{A}_\lambda \boldsymbol{G})) = 2D$ and $\operatorname{Det}(\operatorname{sym}(\mathbf{A}_\lambda \boldsymbol{G})) = D^2 - C^2 - F^2$ we obtain $D > 0$, $D^2 > C^2 - F^2$. If an isotropic scale exists, then we may take $\mathbf{A}_\lambda = \mathbf{1}$, and this condition simplifies to $d > 0$, $d^2 - c^2 - f^2$ (a restriction on only G; see Eq. (6)). See Pecknold et al. (1997a) for the non-crossing condition when the balls are described as fourth order polynomials.

References

Fox, C.G., Hayes, D., 1985. Quantitative methods for analyzing the roughness of the sea floor. Reviews of Geophysics 23, 1–48.

Lavallée, D., Lovejoy, S., Schertzer, D., Ladoy, P., 1993. Nonlinear variability and landscape topography: analysis and simulation. In: De Cola, L., Lam, N. (Eds.), Fractals in Geography. Prentice-Hall, Englewood Cliffs, New Jersey, pp. 171–205.

Lewis, G.M., 1993. The scale invariant generator technique and scaling anisotropy in geophysics. M.Sc. thesis, McGill University, Montreal, Que. 120 pp.

Lovejoy, S., Schertzer, D., 1985. Generalized scale invariance and fractal models of rain. Water Resources Research 21 (8), 1233–1250.

Lovejoy, S., Schertzer, D., 1990. Our multifractal atmosphere: a unique laboratory for non-linear dynamics. Canadian Journal of Physics 46, 62.

Lovejoy, S., Schertzer, D., 1995. How bright is the coast of Brittany? In: Wilkinson, G. (Ed.), Fractals in Geoscience and Remote Sensing. Office for Official Publications of the European Communities, Luxembourg, pp. 102–151.

Lovejoy, S., Schertzer, D., Pflug, K., 1992. Generalized scale invariance and differentially rotating cloud radiances. Physica A 185, 121–127.

Lovejoy, S., Schertzer, D., Silas, P., Tessier, Y., Lavallée, D., 1993. The unified scaling model of atmospheric dynamics and systematic analysis in cloud radiances. Annales Geophysicae 11, 119–127.

Lovejoy, S., Schertzer, D., Tsonis, A.A., 1987. Functional box-counting and multiple dimensions in rain. Science 235, 1036–1038.

Marsan, D., Schertzer, D., Lovejoy, S., 1996. Causal space–time multifractal processes: predictability and forecasting of rain fields. Journal of Geophysical Research 31D, 26333–26346.

Pecknold, S., Lovejoy, S., Schertzer, D., 1997a. The morphology and texture of anisotropic multifractals using generalized scale invariance. In: Woyczynski, W., Molchansov, S. (Eds.), Stochastic Models in Geosystems. Springer-Verlag, New York, pp. 269–312.

Pecknold, S., Lovejoy, S., Schertzer, D., Hooge, C., 1997b. Multifractals and the resolution dependence of remotely sensed data: generalized scale invariance and geographical information systems. In: Quattrochi, M.G.D. (Ed.), Scaling in Remote Sensing and Geographical Information Systems. Lewis, Boca Raton, Florida, pp. 361–394.

Pecknold, S., Lovejoy, S., Schertzer, D., Hooge, C., Malouin, J.F., 1993. The simulation of multifractals. In: Perdang, J.M., Lejeune, A. (Eds.), Cellular Automata: Prospects in Astronomy and Astrophysics. World Scientific, Singapore, pp. 228–267.

Pflug, K., Lovejoy, S., Schertzer, D., 1991. Generalized scale invariance, differential rotation and cloud texture. In:

Sagdeev, R.Z., Frisch, U., Moiseev, A.S., Erokhin, A. (Eds.), Nonlinear Dynamics of Structures. World Scientific, Singapore, pp. 72–78.

Pflug, K., Lovejoy, S., Schertzer, D., 1993. Generalized scale invariance, differential rotation and cloud texture. Journal of the Atmospheric Sciences 50, 538–553.

Pilkington, M., Todoeschuk, J.P., 1993. Fractal magnetization of continental crust. Geophysical Research Letters 20 (7), 627–630.

Press, W.H., Flannery, B.P., Teukolsky, S.A., Vetterling, W.T., 1986. Numerical Recipes: The Art of Scientific Computing. Cambridge University Press, New York, 888 pp.

Schertzer, D., Lovejoy, S., 1983. Elliptical turbulence in the atmosphere. In: Fourth Symposium on Turbulent Shear Flows, Karlshule, Germany.

Schertzer, D., Lovejoy, S., 1984. On the dimension of atmospheric motions. In: Tatsumi, T. (Ed.), Turbulence and Chaotic phenomena in Fluids, IUTAM. Elsevier Science Publishers, New York, pp. 505–512.

Schertzer, D., Lovejoy, S., 1985. Generalised scale invariance in turbulent phenomena. Physico-Chemical Hydrodynamics Journal 6, 623–635.

Schertzer, D., Lovejoy, S., 1987. Physical modeling and analysis of rain and clouds by anisotropic scaling of multiplicative processes. Journal of Geophysical Research 92, 9693–9714.

Schertzer, D., Lovejoy, S., 1989. Nonlinear variability in geophysics: multifractal analysis and simulation. In: Pietronero, L. (Ed.), Fractals: Physical Origin and Consequences. Plenum, New York, p. 49.

Schertzer, D., Lovejoy, S., 1991. Nonlinear geodynamical variability: multiple singularities, universality and observables. In: Schertzer, D., Lovejoy, S. (Eds.), Non-Linear Variability in Geophysics: Scaling and Fractals. Kluwer, Dordrecht, pp. 41–82.

Schertzer, D., Lovejoy, S., Schmitt, F., Chigirinskaya, Y., Marsan, D., 1997. Multifractal cascade dynamics and turbulent intermittency. Fractals 5, 427–471.

Schmitt, F., Lovejoy, S., Schertzer, D., 1995. Multifractal analysis of the Greenland ice-core project climate data. Geophysical Research Letters 22, 1689–1692.

Schmitt, F., Lovejoy, S., Schertzer, D., Lavallée, D., Hooge, C., 1992. First estimates of multifractal indices for velocity and temperature fields. Comptes Rendus de l'Academie des Sciences de Paris, serie II 314, 749–754.

Schmitt, F., Schertzer, D., Lovejoy, S., Brunet, G., 1996. Universal multifractal structure of atmospheric temperature and velocity fields. Europhysics Letters 34, 195–200.

Tessier, Y., Lovejoy, S., Schertzer, D., 1993. Universal multifractals: theory and observations for rain and clouds. Journal of Applied Meteorology 32 (2), 223–250.

VanZandt, T.E., Smith, S.A., Tsuda, T., Fritts, D.C., Sato, T., Fukao, S., Kato, S., 1990. Studies of velocity fluctuations in the lower atmosphere using MU radar. Part I. Azimuthal anisotropy. Journal of the Atmospheric Sciences 47, 39–50.

Wilson, J., Schertzer, D., Lovejoy, S., 1991. Physically based modelling by multiplicative cascade processes. In: Schertzer, D., Lovejoy, S. (Eds.), Non-Linear Variability in Geophysics: Scaling and Fractals. Kluwer, Dordrecht, pp. 185–208.